An Analytical Framework for Midlatitude Temperature Variability with Diabatic Heating and Finite Correlation Time

Keiko Kircher, Ryan L. Sriver, Cristian Proistosescu

Department of Climate, Meteorology and Atmospheric Sciences
University of Illinois at Urbana-Champaign
1301 W Green St, Urbana, IL 61801, U.S.A.

Key Points:

- Analytical expressions for the non-Gaussian statistical moments of atmospheric temperature with explicit diabatic effects are derived
- Temperature moments depend solely on Gaussian wind statistics, a thermal relaxation time and the mean temperature profile
- Framework offers an efficient diagnostic tool that remains valid for predicting extremes even in non-stationarity conditions

Corresponding author: Keiko Kircher, keikoino@illinois.edu

Abstract

We present an analytical framework for calculating the first four statistical moments of the atmospheric temperature distribution, including advection and diabatic effects via the stochastic advection equation under a Gaussian wind and a Newtonian relaxation approximation. While this equation has been previously solved numerically, analytical expressions for these moments have yet to be established. Here, we derive the closed-form expressions for the moments of the atmospheric temperature distribution with the statistical properties of the Gaussian wind, the relaxation time, and the time-mean temperature. Our theory explains previous theoretical, numerical, and empirical frameworks and incorporates diabatic effects. The findings offer a computationally efficient method for calculating temperature moments, based on first-principles physics. The framework provides a physical understanding of the general mechanisms (including diabatic effects) controlling temperature distributions that is valid even in non-stationarity conditions.

Plain Language Summary

Predicting the frequency of extreme temperature events requires understanding not just the mean and variance of the atmospheric temperature distribution, but also higher-order moments, most importantly, skewness and kurtosis. Due to mathematical complexity, calculations of skewness and kurtosis incorporating diabatic (non-adiabatic) heat transfer have traditionally been limited to numerical simulations. This paper presents analytical expressions for the first four statistical moments (mean, variance, skewness, and kurtosis) of the atmospheric temperature distributions that include an explicit description of diabatic heat transfer. These expressions depend on simple statistical properties of the meridional wind, characteristic timescales of the wind persistence and thermal relaxation, and the Earth's time-mean temperature profile. As a result, unlike traditional methods that require extensive runtime on powerful computers, our framework calculates skewness and kurtosis much more efficiently. Furthermore, our explicit, closed-form expressions can be used as a benchmark to check if models are capturing the essential large-scale properties. Most importantly, our framework works even when the Earth's state parameters change over time; while traditional computer simulations become much more complicated and time-consuming under shifting conditions, our math-based method remains fast and straightforward because it requires only substitution of values to the equations.

1 Introduction

Estimating the statistical moments of the atmospheric temperature distribution is a long-standing challenge in the atmospheric sciences. Because empirical observations indicate that midlatitude atmospheric temperature distributions exhibit non-Gaussian behavior (White, 1980; Trenberth & Mo, 1985; Nakamura & Wallace, 1991; Holzer, 1996; Screen, 2014; Cavanaugh & Shen, 2014), accurately quantifying the frequency and intensity of extreme temperature events requires an understanding of higher-order moments such as skewness and kurtosis. To calculate these moments, General Circulation Models (GCMs) (Huth et al., 2003; Haugen et al., 2018) and observational datasets (Shen et al., 2011; McKinnon et al., 2016; Loikith et al., 2018; Loikith & Neelin, 2019) are widely used to extract the moments directly. As a less computationally intensive alternative, Linz et al. (2018) numerically solved the advection-diffusion equation with Newtonian relaxation to understand how the temperature distribution changes with variations in thermal relaxation and eddy stirring. Furthermore, Linz et al. (2020) numerically diagnosed the effect of each term in the advection-diffusion equation on the shape of the atmospheric temperature distribution.

Parallel to these numerical treatments, several studies have sought analytical approaches. Developing analytical frameworks presents clear advantages, as they (1) pro-

vide quantitative insight into model structure beyond what qualitative numerical plots can offer, thereby facilitating sensitivity analyses; (2) serve as a benchmark for limiting case verification, ensuring the reliability of numerical algorithms; and (3) enable computationally efficient moment calculations, significantly reducing processing time. Schneider et al. (2015) demonstrated how to calculate the variance of temperature from the time-mean temperature, assuming that the anomalies are driven by advection of the mean profile, while Tamarin-Brodsky et al. (2020) derived an approximate equation for skewness using only local average absolute intensities of cold and warm anomalies, and Tamarin-Brodsky et al. (2022) derived an approximate equation for excess kurtosis by approximating the original distribution function with a superposition of three Gaussian distributions. Kircher et al. (2025) generalized these concepts to derive a comprehensive analytical framework for statistical moments of arbitrary order, establishing a unified theoretical point of origin. However, while these studies have advanced the analytical formulations of non-Gaussian atmospheric temperature distributions, they could not explicitly account for the effects of diabatic heating and cooling. Even in the generalized theory presented by Kircher et al. (2025), diabatic effects were not included. In their kinematic model, the "source temperature" serves as the starting point of their theory, but it is determined by external physical processes—including diabatic mechanisms—that lie beyond the scope of their theory.

Here, we present an analytical framework to calculate the first four atmospheric temperature moments in the midlatitude lower troposphere that incorporates diabatic effects. Our closed-form expressions express these moments as functions of the spatial derivatives of the time-mean temperature, the variance of the velocity of the Gaussian wind, the characteristic correlation time of the air parcels, and the characteristic relaxation time of diabatic effects. We demonstrate that our theoretical framework successfully unifies prior analytical frameworks, explains past numerical frameworks with explicit mathematical expressions, and exhibits strong agreement with observations and idealized aquaplanet simulations using Isca model (Vallis et al., 2018) under a Held-Suarez configuration (Held & Suarez, 1994). While numerical models and observational datasets require massive temporal sampling to overcome statistical noise in higher-order moments—making them highly sensitive to individual outliers and sampling limitations—our framework circumvents this computational burden by enabling the direct estimation of higher-order moments solely from the time-mean temperature profile with minimal computational cost. However, the primary objective of this framework is not to compete with complex numerical models in predictive precision, but to establish an analytical theory derived from first-principles physics that provides a conceptual understanding that numerical simulations cannot offer, such as scaling laws that explain midlatitude temperature variability.

2 Theoretical Framework

To calculate the statistical moments of atmospheric temperature distributions, we utilize the framework presented by Kircher et al. (2026) for evaluating single-point statistical moments of a stochastic advection equation with linear relaxation, mapping it directly to tropospheric temperature. In their model, the closed-form expressions for single-point statistical moments were derived for the solution of a nonhomogeneous stochastic advection equation with linear relaxation. With the use of atmospheric variables, the governing equation for temperature $T(\phi, t)$ at time t and latitude ϕ is

$$\frac{\partial T(\phi,t)}{\partial t} + v(t)\frac{\partial T(\phi,t)}{\partial \phi} = -\frac{T(\phi,t) - T_e(\phi)}{\tau}, \tag{1}$$

where $v(t)$ is the stochastic velocity following a Gaussian distribution with zero mean, $T_e(\phi)$ is the equilibrium temperature profile, and τ is the characteristic time scale of diabatic effects. This equation describes the temperature advection of an idealized midlatitude lower troposphere; temperature $T(\phi, t)$ is advected by a stochastic meridional

wind $v(t)$, arising from the abundant eddy activity in the midlatitude troposphere, and the temperature continuously relaxes to its time-independent equilibrium profile due to diabatic (mostly radiative) effects. Following their derivation, solving Eq. (1) yields the first four single-point statistical moments directly from the time-mean state of the temperature, where the second, third, and the fourth central moments in terms of the time-mean temperature $\bar{T}$ are given by

$$\sigma_T^2 = \bar{T}'^2 \sigma_\phi^2 \tag{2}$$

$$\mu_3 = 4\bar{T}'' \sigma_\phi^2 \sigma_T^2 \tag{3}$$

$$\mu_4 = \left(3 + \frac{13}{8}\alpha_3^2 + 4\bar{T}'\bar{T}^{(3)}\frac{\sigma_\phi^4}{\sigma_T^2}\right)\sigma_T^4, \tag{4}$$

where $\alpha_3 = \mu_3/\sigma_T^3$ is skewness (normalized third moment), a prime indicates the derivative with latitude ϕ,

$$\sigma_\phi^2 = \frac{1}{2}\sigma_v^2 \Delta t \tau, \tag{5}$$

and σ_v^2 is the variance of the stochastic wind $v(t)$, and Δt is a characteristic correlation time. Mathematically, $\sigma_\phi^2 = \sigma_v^2 \Delta t \tau/2$ represents the average variance of the distance traveled during a one-dimensional random walk with a step size of $\sigma_v \Delta t$ over a time τ. Physically, σ_ϕ describes the average root-mean-square distance a fluid parcel travels before its thermal properties get reset by relaxation. When applied to an atmosphere, the physical interpretation of σ_ϕ is analogous to that of the classical eddy mixing length—the average distance a turbulent fluid parcel travels before losing its properties. However, it differs from the classic expression $l_{eddy} = u'\tau$, where u' represents the fluctuation velocity. In the classic case, a fluid parcel is assumed to maintain a constant velocity u' throughout the entire time τ until it equilibrates with the environment. In contrast, our theory considers a more realistic view of the fluid parcels, where each parcel undergoes multiple velocity changes before it equilibrates.

While the first moment is omitted above because it is simply $\bar{T} = \bar{T}$, the expression of $\bar{T}$ in terms of T_e shows how mean temperature differs from the equilibrium profile:

$$\bar{T} = T_e + T_e'' \sigma_\phi^2. \tag{6}$$

Even though moments can be expressed in terms of T_e, Eq. (6) is used to express the moments in terms of $\bar{T}$ because while T_e is not directly observable, it is significantly easier to calculate $\bar{T}$ from observational and simulation datasets. Equations (2)–(4) show that variance is proportional to the relaxation time τ and is proportional to the square of the first derivative $\bar{T}'$, skewness is proportional to the square root of the relaxation time $\sqrt{\tau}$ and is proportional to $\bar{T}''$, and excess kurtosis is proportional to the relaxation time τ and incorporates $\bar{T}'$, $\bar{T}''$, and $\bar{T}^{(3)}$. To show that Eqs. (2)–(4) are applicable as approximate statistical moments of temperature in midlatitude lower troposphere on the Earth, we first note that temperature fluctuations in the Earth's troposphere are small relative to the magnitude of temperature, which makes the advection equation with Newtonian relaxation approximation an appropriate representation of radiative heating and cooling in regimes where nonlinear diabatic heating, such as latent heat release, is negligible (Sellers, 1969; Budyko, 1969; Held & Suarez, 1994; Linz et al., 2018, 2020; Zhang et al., 2022).

In addition, the derivation of Eqs. (2)–(4) by Kircher et al. (2026) was performed under the following asymptotic condition: the length scale of the spatial change in the n^{th} derivative of the equilibrium profile is much larger than the typical distance the air

parcel moves within Δt; that is,

$$v(t)\Delta t \ll \left| \frac{d^n T_e(\phi)/d\phi^n}{d^{n+1} T_e(\phi)/d\phi^{n+1}} \right|, \; n = 1, 2, \ldots \tag{7}$$

on average. In Earth's midlatitude lower troposphere, the mixing length $L' = R_E \sigma_v \Delta t \sim$ 900 km, where R_E is the radius of the Earth (Taylor, 1922; Bennett, 1987; Daoud et al., 2003; Swanson & Pierrehumbert, 1997), is empirically found to be much smaller than the length scale of the change in temperature $\sim 10^4$ km (Schneider et al., 2015). Hence $\sigma_v \Delta t \sim 0.1$ and

$$\left| \frac{T_e(\phi)}{dT_e(\phi)/d\phi} \right| \sim 1, \tag{8}$$

thus Eq. (7) is valid for $n = 0$. For $n \geq 1$. Since Earth's meridional temperature profile resembles a sinusoidal function in midlatitudes (Feulner et al., 2013), if $T_e(\phi) \sim \cos\phi$, then

$$\left| \frac{d^n T_e(\phi)/d\phi^n}{d^{n+1} T_e(\phi)/d\phi^{n+1}} \right| = \begin{cases} |\tan\phi| \text{ (odd } n) \\ |\cot\phi| \text{ (even } n), \end{cases} \tag{9}$$

both of which are of the order of 1 in midlatitudes. Thus, if Eq.(7) is satisfied with $n = 0$, then it is satisfied for $n \geq 1$ as well. Therefore, Eq. (7) is a good assumption for modeling the Earth's midlatitude lower troposphere, thus, so are Eqs. (2)—(4).

3 Model Validation and Applications

To validate Eqs. (2)–(4) for application to the Earth's midlatitude lower troposphere, we evaluate the prediction made by those equations against previous theories, simulations, and observations. Given the highly idealized nature of our model, these comparisons are intended to validate only the core structural behavior, rather than to demonstrate precise empirical matching.

We begin by comparing the results with the generalized theoretical framework of Kircher et al. (2025). As explained in section 1, this theory has unified prior analytical frameworks without explicit diabatic effects (Schneider et al., 2015; Tamarin-Brodsky et al., 2020, 2022). Therefore, demonstrating that our theoretical framework agrees with their theory establishes a broader consistency across all these theories.

The second, third, and fourth central moments of midlatitude lower troposphere temperature distribution calculated in their theory are:

$$\sigma_T^2 \; = \bar{T}'(\phi)^2 \sigma_\eta^2 \tag{10}$$

$$\mu_3 = 3\bar{T}'' \sigma_\eta^2 \sigma_T^2 \tag{11}$$

$$\mu_4 = \left(3 + \frac{5}{3}\alpha_3^2 + 4\bar{T}'\bar{T}^{(3)} \frac{\sigma_\eta^4}{\sigma_T^2} \right) \sigma_T^4, \tag{12}$$

where σ_η is the standard deviation of the distance in the $\hat{\phi}$ direction traveled by the wind within a characteristic correlation time. Clearly, the expressions of variance—Eq. (2) and Eq. (10)— are identical, provided that $\sigma_\eta = \sigma_\phi$. Recall that $\sigma_\phi^2 = \sigma_v^2 \Delta t \tau / 2$ is the average variance of the distance traveled during a one-dimensional random walk with a step

size of $\sigma_v \Delta t$ over a time τ, and the physical meaning of σ_ϕ is the average root-mean-square distance a fluid parcel travels before its thermal properties get reset by relaxation. This is consistent with the physical interpretation of σ_η in Kircher et al. (2025), which represents the expected distance a Gaussian wind moves before the temperature at a given location gets replaced by the next temperature value. Hence it is reasonable to set $\sigma_\phi^2 = \sigma_v^2 \Delta t \tau/2$. Both third and fourth moments (μ_3 and μ_4) exhibit the same functional dependence on $\bar{T}$ and σ_ϕ, albeit with slightly different numerical factors.

Note that the quantity $\sigma_\phi = (1/\sqrt{2})\sigma_v\sqrt{\tau \Delta t}$ is the only part that contains the information about diabatic effects (i.e., where the parameter τ appears). In Kircher et al. (2025), the quantity σ_ϕ is an external parameter. Through the expression $\sigma_\phi = (1/\sqrt{2})\sigma_v\sqrt{\tau \Delta t}$, our current theory explicitly shows how diabatic effects are integrated into this framework.

Our theoretical framework can explain previous numerical studies that include diabatic heating as well. In Linz et al. (2018), the advection equation with Newtonian relaxation was solved numerically to evaluate the impacts on the temperature probability density function with various thermal relaxation time scale and location of the eddy stirring. Their results demonstrate that an increase in τ leads to a corresponding increase in variance, while exerting a lesser influence on skewness when nothing else is varied. Within our theoretical framework, variance scales as τ, whereas skewness $\alpha_3 = \mu_3/\sigma_T^3$ is proportional to $\sqrt{\tau}$; these scaling laws are consistent with their observations, both regarding the increase in variance and the relatively lower sensitivity of skewness to changes in τ compared to variance when everything else stays constant.

In addition to the numerical analysis by Linz et al. (2018), we compare our theory with output data from idealized aquaplanet Isca simulations (Vallis et al., 2018) using a Held-Suarez configuration (Held & Suarez, 1994). In the kinematic model of Kircher et al. (2025), the variance of the distance traveled by the Gaussian stochastic wind within a characteristic time is treated as an external parameter. Thus, when comparing their model to the Isca dataset, they needed to determine this quantity by matching the theoretical and simulated temperature variances. In contrast, our current framework eliminates the need for such fitting, as we can predict the unfitted variance of the wind velocity via Eq. (5) by calculating τ and Δt from temperature and meridional wind velocity data. In particular, σ_v, the standard deviation of the meridional wind velocity field, is calculated directly from the meridional velocity data at each grid, and τ and Δt are calculated via

$$\tau = \left| \frac{T}{dT/dt} \right| \tag{13}$$

$$\Delta t = \left| \frac{v}{dv/dt} \right| \tag{14}$$

respectively using temperature and meridional velocity data. The approximate values from the data ($\sqrt{\overline{f^2}/\overline{(df/dt)^2}}$, $f \in \{T, v\}$) are calculated at each grid and averaged with time for the calculation of σ_ϕ for each grid. To calculate $\bar{T}$, we find the time average of temperature at each grid. Derivative of $\bar{T}$ in the meridional direction is taken to calculate $\bar{T}'$. Since the simulation uses an aquaplanet, we pick one longitude (longitude = 0 degrees) to plot the standard deviation as a representative. An identical analysis was conducted at other longitudes, but it yielded no physically significant differences. Figure 1 demonstrates the agreement between the Isca simulation data and our theoretical prediction for σ_T at that representative longitude, especially in the lower midlatitudes. This validation, which was impossible in Kircher et al. (2025), provides a further justification for their previous results and the effectiveness of our current theory.

The validation of our framework against observations is demonstrated transitively through its consistency with Linz et al. (2018), which itself matches ERA5 data for both

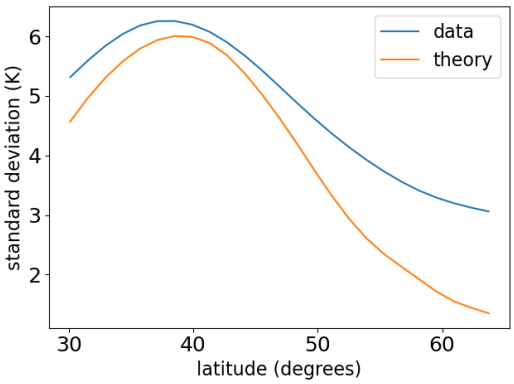


Figure 1. Standard deviation of the temperature distribution. Blue line shows the values calculated directly from Isca data at a given longitude, and the orange line shows the values calculated from $\bar{T}$, τ, Δt, and σ_v via our analytical framework.

variance and skewness.

(15)

However, to provide a direct validation of our framework against the real-world atmosphere, we compare the statistical properties of temperature calculated directly from data and those calculated from our theory. In particular, we compare the observational and theoretical values of zonally-averaged standard deviation, skewness, and kurtosis using ERA5 surface data from 1985 to 2014 in the months of January. We use the same method to avoid numerical instabilities as in the Isca case (also as in Kircher et al. (2025)). As such, values of $\bar{T}'$, σ_v, τ, and Δt are calculated in the same way as the Isca case, except we take 4-day averages for Δt (exact same approximation as ISCA shows similar final results as shown in Figure S1). The zonal averages of the moments are taken after the calculation of the moments at each longitude rather than calculating the moments from the zonally-averaged temperature. Figure 2 demonstrates the agreements in zonal averages of standard deviation, skewness, and excess kurtosis, where the blue lines show the values calculated directly from the dataset, the orange lines show the values calculated via our theory, and the yellow lines show the theoretical values calculated with 30 individual Januaries to show the year-to-year variability in the estimates. In each case, the data and theory agree well in the Southern Hemisphere midlatitudes and the variability increases with the order of moments due to the increasing sensitivity in Δt and τ, which contain the largest sources of variability. Figure 3 and Figure 4 show global maps of standard deviation and skewness in the lower troposphere over 30 years for the month of January, using ERA5 daily data ($\bar{T}'$, σ_v, τ, and Δt are calculated at each grid as before; see Figure S2 and S3 for the case where all variables are approximated as done in the case of Isca). In each figure, the left panel shows the quantity calculated directly from the data, and the right panel shows the same quantity derived from our theory using the mean temperature profile $\bar{T}$. The two plots show good agreement, especially in midlatitudes of the Southern Hemisphere. This region has abundant meridional mixing and is predominantly ocean surface.; the lower surface roughness of the ocean closely matches the idealized model assumptions in Sec. 2, as the lack of topographic obstacles allows the wind to maintain a nearly Gaussian distribution. On the other hand, the discrepancy between data and theory is much larger in areas with large topographic features such as mountain ranges. This is likely due to the fact that meridional wind cannot be Gaussian in these regions. In addition to topographic effects, prediction of the statistical moments with our theory deviates from the observation in higher latitudes along storm

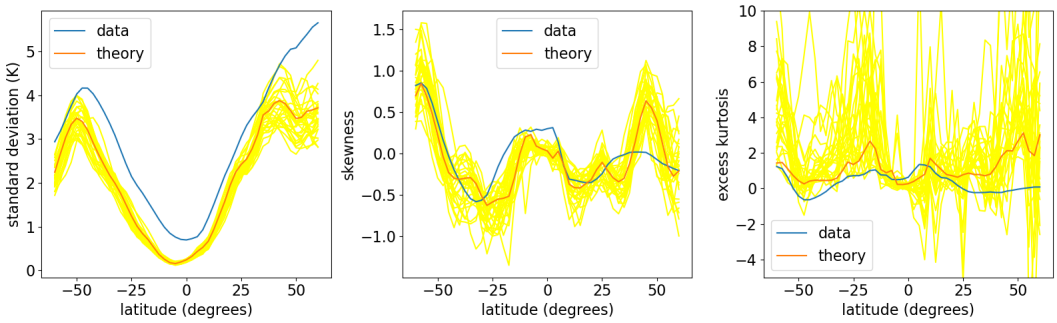


Figure 2. Zonal average values of standard deviation, skewness, and kurtosis of atmospheric surface temperature as functions of latitude. The blue lines show the values calculated directly from ERA5 surface data from 1985 to 2014 in the months of January, and the orange lines show the values calculated from $\bar{T}$, τ, Δt, and σ_v via our analytical framework. Yellow lines show theoretical values calculated from 30 individual Januaries for the period 1985-2014.

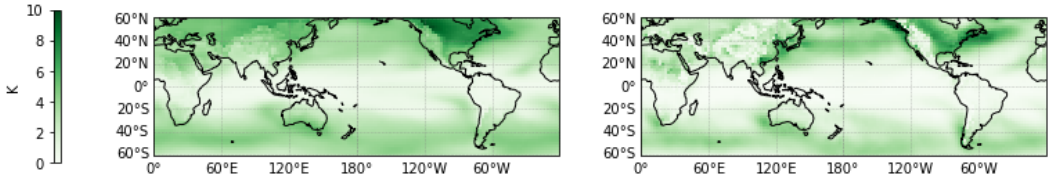


Figure 3. Standard deviation of the atmospheric surface temperature distribution. The plot on the left shows σ_T calculated directly from ERA5 surface data from 1985 to 2014 in the months of January. The plot on the right shows σ_T calculated from mean temperature profile $\bar{T}$, τ, Δt, and σ_v via our analytical framework.

tracks as well. As seen in Figure 5, these areas coincide with the areas where Eq.(7) is not satisfied (see Figure S4 for the case where Δt is approximated the same way as in Isca).

4 Discussion and Conclusions

In this work, we have shown closed-form expressions for the first four statistical moments of atmospheric temperature in the midlatitude lower troposphere. The model includes advection of temperature by a Gaussian stochastic meridional wind and diabatic heat transfer via Newtonian relaxation. The moments are expressed as functions of characteristic correlation time, variance of the Gaussian wind, characteristic relaxation time of air parcels, and time-mean temperature. Specifically, variance scales linearly with the relaxation time τ and is proportional to the square of the first derivative $\bar{T}'$, skewness scales with a square root of the relaxation time $\sqrt{\tau}$ and is proportional to $\bar{T}''$, and excess kurtosis scales linearly with the relaxation time τ and incorporates $\bar{T}'$, $\bar{T}''$, and $\bar{T}^{(3)}$. By describing these higher-order moments with such macroscopic variables, this framework offers a quantitative understanding of how large-scale physics affects local temperature statistics. Our framework demonstrates strong consistency with simulations and observations, validated both transitively through agreement with prior verified theories and directly via idealized Isca simulations and ERA5 reanalysis datasets.

A primary contribution of this theory is the explicit closed-form expressions of statistical moments of atmospheric temperature that incorporates diabatic effects, which

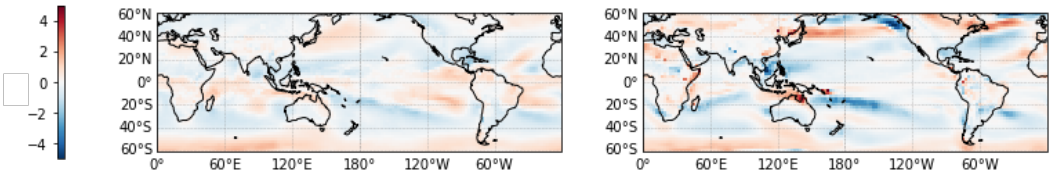


Figure 4. Skewness of the atmospheric surface temperature distribution. The plot on the left shows μ_3 calculated directly from ERA5 surface data from 1985 to 2014 in the months of January. The plot on the right shows μ_3 calculated from mean temperature profile $\bar{T}$, τ, Δt, and σ_v via our analytical framework.

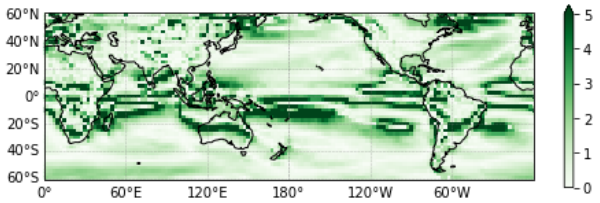


Figure 5. The ratio $\sigma_v \Delta t/((dT/d\phi)/(d^2T/d\phi^2))$ for ERA5 surface data from 1985 to 2014 in the months of January. Regions with large ratio (where Eq. (7) is not satisfied) coincide with where observational data does not match our theory.

was previously accessible only through numerical approximations or empirical heuristics. Unlike purely numerical approaches, where the relationship between thermal relaxation and higher-order moments must be inferred via an empirical fit, our closed-form expressions establish an explicit scaling laws on the diabatic timescale τ. In addition, while in numerical analyses the time-dependence of the parameters of the state of the Earth vastly increases computation time and requires additional computational steps, our framework remains fully applicable exactly the way described in this manuscript even when the Earth's parameters change in time. While the foundational value of this framework—also the primary advancement from Kircher et al. (2025)—lies in its derivation of mid-latitude atmospheric temperature moments from first-principles physics, it simultaneously yields practical advantages. The inclusion of diabatic heat transfer, for example, permits an analysis of thermal transport and the calculation of the characteristic displacement scale of temperature advection.

In the context of atmospheric dynamics, our framework corresponds to a synoptic-scale theory predicated on a Gaussian meridional wind distribution with a zero mean. This characterization is most applicable to regions characterized by abundant synoptic eddies or minimal topographic forcing, or to the free troposphere where surface features do not significantly perturb the flow. As it is an idealized model, when utilizing our results to represent the generalized behavior of statistical moments in specific applications, it is essential to ensure that the underlying assumptions such as a one-dimensional flow, a Gaussian meridional wind profile, Newtonian relaxation and length scale condition (i.e., Eq. (7)) remain valid. Indeed, while our theory provides reasonable estimates of statistical moments, the meridional wind profile deviates from a Gaussian distribution in various locations (see S5 for Jarque-Bera statistics of meridional wind field). This contributes to the observed differences between the theoretical predictions and empirical data. Furthermore, our model assumes that the meridional wind is stochastically time-dependent but spatially uniform, despite evidence suggesting that spatial dependence may be a critical factor in temperature variability (Zhang et al., 2022). Finally, we assume that the

equilibrium temperature and radiative relaxation timescale remain temporally invariant on synoptic timescales. In scenarios where these parameters fluctuate significantly—such as during seasonal transitions (spring or fall) or persistent blocking events such as heat domes—the applicability of the current theory is limited.

Future research includes extending the theory to include transport velocities dependent on both time and space, motivated by the physical significance of vertical transport processes. More prediction-oriented future research includes the inclusion of more physical phenomena such as heat domes, and the development of more precise estimates of τ and Δt for better predictions of temperature moments.

Open Research Section

ERA5 atmospheric reanalysis data are provided by Copernicus Climate Change Service (C3S) (2017): ERA5: Fifth generation of ECMWF atmospheric reanalyses of the global climate . Copernicus Climate Change Service Climate Data Store (CDS), summer 2025. This can be found at doi: 10.1002/qj.3803 (Hersbach et al., 2020). The code for calculating moments from Isca and ERA5 data is available at Zenodo (Kircher, 2026). The code for the ISCA climate model is publicly available and is described at https://doi.org/10.5281/zenodo.21498725.

Conflict of Interest disclosure

The authors declare there are no conflicts of interest for this manuscript.

Acknowledgments

This work was supported by the U.S. Department of Energy, Office of Science, Biological and Environmental Research Program, Earth and Environmental Systems Modeling, MultiSector Dynamics under Cooperative Agreement DE-SC0022141. Any opinions, findings, and conclusions or recommendations expressed in this material are those of the authors and do not necessarily reflect the views of the funding agencies. We thank Neutrina Kircher for her unwavering canine companionship and support. During the preparation of this manuscript, the authors used Google Gemini to correct grammar and improve the flow of the text. The final text was reviewed, edited, and approved by the authors, who take full responsibility for the accuracy and integrity of the content.

References

Bennett, A. F. (1987). A lagrangian analysis of turbulent diffusion. *Reviews of Geophysics*, *25*(4), 799–822.

Budyko, M. I. (1969). The effect of solar radiation variations on the climate of the earth. *tellus*, *21*(5), 611–619.

Cavanaugh, N. R., & Shen, S. S. (2014). Northern hemisphere climatology and trends of statistical moments documented from ghcn-daily surface air temperature station data from 1950 to 2010. *Journal of climate*, *27*(14), 5396–5410.

Daoud, W. Z., Kahl, J. D. W., & Ghorai, J. K. (2003). On the synoptic-scale lagrangian autocorrelation function. *J. Appl. Meteor.*, *42*, 318–324.

Feulner, G., Rahmstorf, S., Levermann, A., & Volkwardt, S. (2013). On the origin of the surface air temperature difference between the hemispheres in earth's present-day climate. *Journal of climate*, *26*(18), 7136–7150.

Haugen, M. A., Stein, M. L., Moyer, E. J., & Sriver, R. L. (2018). Estimating changes in temperature distributions in a large ensemble of climate simulations using quantile regression. *Journal of CLIMATE*, *31*(20), 8573–8588.

Held, I. M., & Suarez, M. J. (1994). A proposal for the intercomparison of the dy-

namical cores of atmospheric general circulation models. *Bulletin of the American Meteorological society*, *75*(10), 1825–1830.

Hersbach, H., Bell, B., Berrisford, P., Hirahara, S., Horányi, A., Muñoz-Sabater, J., ... Thépaut, J.-N. (2020). The era5 global reanalysis. *Quarterly Journal of the Royal Meteorological Society*, *146*(730), 1999-2049. Retrieved from `https://rmets.onlinelibrary.wiley.com/doi/abs/10.1002/qj.3803` doi: https://doi.org/10.1002/qj.3803

Holzer, M. (1996). Asymmetric geopotential height fluctuations from symmetric winds. *Journal of the atmospheric sciences*, *53*(10), 1361–1379.

Huth, R., Kyselỳ, J., & Dubrovskỳ, M. (2003). Simulation of surface air temperature by gcms, statistical downscaling and weather generator: higher-order statistical moments. *Studia Geophysica et Geodaetica*, *47*(1), 203–216.

Kircher, K. (2026, October). *Grl_kircher_2.* Zenodo. Retrieved from `https://doi.org/10.5281/zenodo.23426330` doi: 10.5281/zenodo.23426330

Kircher, K., Proistosescu, C., & Sriver, R. L. (2025). Analytical model for the higher order moments of midlatitude atmospheric temperature distributions. *Geophysical Research Letters*, *52*(3), e2024GL111626.

Kircher, K., Proistosescu, C., & Sriver, R. L. (2026). *Single-point statistical moments of the nonhomogeneous stochastic advection equation in the small correlation length limit.* Retrieved from `https://arxiv.org/abs/2606.29479`

Linz, M., Chen, G., & Hu, Z. (2018). Large-scale atmospheric control on non-gaussian tails of midlatitude temperature distributions. *Geophysical Research Letters*, *45*(17), 9141–9149.

Linz, M., Chen, G., Zhang, B., & Zhang, P. (2020). A framework for understanding how dynamics shape temperature distributions. *Geophysical Research Letters*, *47*(4), e2019GL085684.

Loikith, P. C., & Neelin, J. D. (2019). Non-gaussian cold-side temperature distribution tails and associated synoptic meteorology. *Journal of Climate*, *32*(23), 8399–8414.

Loikith, P. C., Neelin, J. D., Meyerson, J., & Hunter, J. S. (2018). Short warm-side temperature distribution tails drive hot spots of warm temperature extreme increases under near-future warming. *Journal of Climate*, *31*(23), 9469–9487.

McKinnon, K. A., Rhines, A., Tingley, M. P., & Huybers, P. (2016). The changing shape of northern hemisphere summer temperature distributions. *Journal of Geophysical Research: Atmospheres*, *121*(15), 8849–8868.

Nakamura, H., & Wallace, J. M. (1991). Skewness of low-frequency fluctuations in the tropospheric circulation during the northern hemisphere winter. *Journal of Atmospheric Sciences*, *48*(12), 1441–1448.

Schneider, T., Bischoff, T., & Płotka, H. (2015). Physics of changes in synoptic midlatitude temperature variability. *Journal of Climate*, *28*(6), 2312–2331.

Screen, J. A. (2014). Arctic amplification decreases temperature variance in northern mid-to high-latitudes. *Nature Climate Change*, *4*(7), 577–582.

Sellers, W. D. (1969). A global climatic model based on the energy balance of the earth-atmosphere system. *Journal of Applied Meteorology (1962-1982)*, 392–400.

Shen, S. S., Gurung, A. B., Oh, H.-S., Shu, T., & Easterling, D. R. (2011). The twentieth century contiguous us temperature changes indicated by daily data and higher statistical moments. *Climatic Change*, *109*(3), 287–317.

Swanson, K. L., & Pierrehumbert, R. T. (1997). Lower-tropospheric heat transport in the pacific storm track. *J. Atmos. Sci.*, *54*, 1533–1543.

Tamarin-Brodsky, T., Hodges, K., Hoskins, B. J., & Shepherd, T. G. (2020). Changes in northern hemisphere temperature variability shaped by regional warming patterns. *Nature Geoscience*, *13*(6), 414–421.

Tamarin-Brodsky, T., Hodges, K., Hoskins, B. J., & Shepherd, T. G. (2022). A simple model for interpreting temperature variability and its higher-order changes.

Journal of Climate, *35*(1), 387–403.

Taylor, G. I. (1922). Diffusion by continuous movements. *Proceedings of the london mathematical society*, *2*(1), 196–212.

Trenberth, K. F., & Mo, K. C. (1985). Blocking in the southern hemisphere. *Monthly Weather Review*, *113*(1), 3–21.

Vallis, G. K., Colyer, G., Geen, R., Gerber, E., Jucker, M., Maher, P., ... Thomson, S. I. (2018). Isca, v1.0: a framework for the global modelling of the atmospheres of earth and other planets at varying levels of complexity. *Geoscientific Model Development*, *11*(3), 843–859. Retrieved from `https://gmd.copernicus.org/articles/11/843/2018/` doi: 10.5194/gmd-11-843-2018

White, G. H. (1980). Skewness, kurtosis and extreme values of northern hemisphere geopotential heights. *Monthly Weather Review*, *108*(9), 1446–1455.

Zhang, B., Linz, M., & Chen, G. (2022). Interpreting observed temperature probability distributions using a relationship between temperature and temperature advection. *Journal of Climate*, *35*(2), 705–724.